

High-resolution X-ray spectroscopy of θ Carinae^{*}

Y. Nazé^{**} and G. Rauw^{***}

Institut d'Astrophysique et de Géophysique, Université de Liège, Allée du 6 août 17, Bât. B5C, 4000 Liège, Belgium
e-mail: naze@astro.ulg.ac.be

Received 10 June 2008 / Accepted 21 August 2008

ABSTRACT

Context. The peculiar hot star θ Car in the open cluster IC 2602 is a blue straggler as well as a single-line binary with a short period (2.2d).

Aims. Its high-energy properties are not well known, though X-rays can provide useful constraints on the energetic processes at work in binaries as well as in peculiar, single objects.

Methods. We present the analysis of a 50 ks exposure taken with the XMM-Newton observatory. It provides medium as well as high-resolution spectroscopy.

Results. Our high-resolution spectroscopy analysis reveals a very soft spectrum with multiple temperature components (1–6 MK) and an X-ray flux slightly below the ‘canonical’ value ($\log [L_X(0.1-10.)/L_{\text{BOL}}] \sim -7$). The X-ray lines appear surprisingly narrow and unshifted, reminiscent of those of β Cru and τ Sco. Their relative intensities confirm the anomalous abundances detected in the optical domain (C strongly depleted, N strongly enriched, O slightly depleted). In addition, the X-ray data favor a slight depletion in neon and iron, but they are less conclusive for the magnesium abundance, which may be solar-like. While no significant changes occur during the XMM-Newton observation, variability in the X-ray domain is detected in the long-term range. The formation radius of the X-ray emission is loosely constrained to $<5 R_\odot$, which allows for a range of models (wind-shock, corona, magnetic confinement, ...) though not all of them can be reconciled with the softness of the spectrum and the narrowness of the lines.

Key words. X-rays: stars – stars: individual: θ Carinae – stars: early-type

1. Introduction

θ Car (=HD 93030) is a luminous star of type B0.2V belonging to the open cluster IC 2602, situated at 152 pc (Robichon et al. 1999). The cluster is 30 Myr old, and the massive, hot θ Car therefore appears to be a rare example of a blue straggler. Its optical spectrum displays hints of enhanced nitrogen (a three-fold enrichment with respect to solar) and depleted carbon (at least by an order of magnitude) and oxygen (a factor of about 1/4, see Hubrig et al. 2008). In addition, θ Car is also a binary system, with a short period (2.2d, Lloyd et al. 1995) and small eccentricity ($e = 0.13$, Hubrig et al. 2008). The companion remains undetected in the visible spectrum (its flux contributes to $<0.1\%$ of the total flux) and should therefore be of a much later spectral type ($M \sim 1 M_\odot$, Hubrig et al. 2008). The binarity and anomalous abundances might suggest that the blue straggler character of θ Car results from a past episode of mass-transfer between these two stars.

Because of its peculiar properties, the spectrum of θ Car has been investigated several times, notably to search for the presence of a magnetic field (Borra & Landstreet 1979; Hubrig et al. 2008). The results are rather inconclusive, but an intriguing period of about 9 min was detected in the most recent spectropolarimetric results.

We further study the star in the high-energy domain. After its detection by Einstein and Rosat, θ Car is known as the brightest

X-ray source of IC 2602, but only approximate X-ray properties have been derived up to now. The current generation of X-ray facilities (Chandra, XMM-Newton) provides detailed insight into the X-ray emission, especially thanks to their grating instruments. However, these observatories have observed only a handful of B stars at high spectral resolution (τ Sco, β Cru, ϵ Ori, Spica) and no blue stragglers. The analysis of θ Car thus nicely fills a gap, and could help us better understand the high-energy characteristics of hot stars.

The paper is organized as follows: the data and reduction processes are presented in Sect. 2, the general properties of θ Car in the X-ray domain are examined in Sect. 3.1, the detailed characteristics of the X-ray lines are derived in Sect. 3.2, and we finally conclude in Sect. 4.

2. X-ray observations

On 2002 Aug. 13 (Rev. 0490, PI R. Pallavicini), the IC 2602 cluster was observed with XMM-Newton for a total exposure time of 50 ks. We retrieved this dataset from the XMM-Newton public archives in order to perform a thorough analysis of the high-energy emission of θ Car. We processed these archival data with the Science Analysis System (SAS) software, version 7.0; further analysis was performed using the FTOOLS tasks and the XSPEC software v 11.2.0.

For this observation, the three European Photon Imaging Cameras (EPICs) were operated in the standard, full-frame mode and a thick filter was used to reject optical light. After application of the pipeline chains (tasks EMPROC, EPPROC), the EPIC data were filtered as recommended by the SAS team: for the EPIC MOS (Metal Oxide Semi-conductor) detectors, we kept

^{*} Based on observations collected with XMM-Newton, an ESA Science Mission with instruments and contributions directly funded by ESA Member States and the USA (NASA).

^{**} Postdoctoral Researcher FNRS.

^{***} Research Associate FNRS.

the single, double, triple and quadruple events (i.e. the pattern between 0 and 12) that pass through the #XMMEA_EM filter; for the EPIC pn detector, only single and double events (i.e. the pattern between 0 and 4) with flag = 0 were considered. To check for contamination by low-energy protons, we have further examined the light curve at high energies (Pulse Invariant channel number $>10\,000$, $E \gtrsim 10$ keV, and with pattern = 0). A large background flare due to soft protons (most probably of solar origin) occurred towards the end of the observation and we therefore discarded time intervals where the lightcurves for PI $> 10\,000$ present an EPIC MOS count rate greater than 0.3 cts s^{-1} and an EPIC pn count rate greater than 1 cts s^{-1} . The pn data of θ Car are severely affected by the presence of CCD gaps and bad columns and we therefore decided to discard them from the present analysis. A circular source region of $50''$ radius and an annular background region of 50 and $90''$ radii (both centered on θ Car) were then used to extract spectra and lightcurves. Due to the brightness of the source, it was not necessary to bin the EPIC MOS spectra, but bad energy bins and noisy bins at $E < 0.15$ keV or >10 keV were discarded.

In this observation, θ Car appears near the center of the field-of-view (FOV) and some information could therefore be recorded with the Reflection Grating Spectrograph (RGS). However, since θ Car was not *exactly* at the center of the FOV, the standard processing could not be used: the pipeline chain (task RGSPROC) had to be run specifically with the coordinates of the object. As for EPIC, a flare in the lightcurve was detected and time intervals presenting an RGS count rate greater than 0.35 cts s^{-1} were therefore discarded. In addition, a relatively bright X-ray source associated with HD 307938 (G0) also appears in the RGS FOV: though it does not contaminate the RGS spectrum of θ Car, it could lead to a wrong estimate of the background and we therefore had to mask this source for the background calculation. For both non-standard operations, we closely followed the recommendations from the SAS team (see the SAS threads on the XMM website). The RGS spectra were binned to reach at least 5 cts per bin and only data between 0.35 and 1.8 keV were considered; the data from the second order contain too few counts to be useful, and we therefore also discarded them from the analysis.

3. High-energy properties of θ Car

3.1. General characteristics

θ Car appears as the brightest X-ray source in the field of IC 2602. The SAS detection algorithm (task EDETECT_CHAIN) indicates that the count rates in the 0.4–10 keV energy band amount to 0.255 ± 0.003 cts s^{-1} for MOS1 and to 0.258 ± 0.003 cts s^{-1} for MOS2 (note that this is still well below the limit for pile-up). In addition, the hardness ratios are very small, revealing the softness of the source: $HR1 = (M-S)/(M+S)$ is -0.720 ± 0.008 for MOS1 and -0.724 ± 0.008 for MOS2, $HR2 = (H-M)/(H+M)$ is -0.920 ± 0.015 for MOS1 and -0.956 ± 0.011 for MOS2 where S, M, and H are the count rates in the soft (0.4–1 keV), medium (1–2 keV) and hard (2–10 keV) energy bands. Finally, the MOS lightcurves in the 0.2–5 keV band were analyzed by χ^2 and *pov* tests (Sana et al. 2004) but no significant variation was detected during the 50 ks observation (Fig. 1, note that this covers about one quarter of the orbit of the spectroscopic binary). We thus decided to analyze the spectral properties derived from the whole observation.

Two types of spectra are available: the EPIC low-resolution ones and the RGS high-resolution ones (Fig. 2). Both datasets

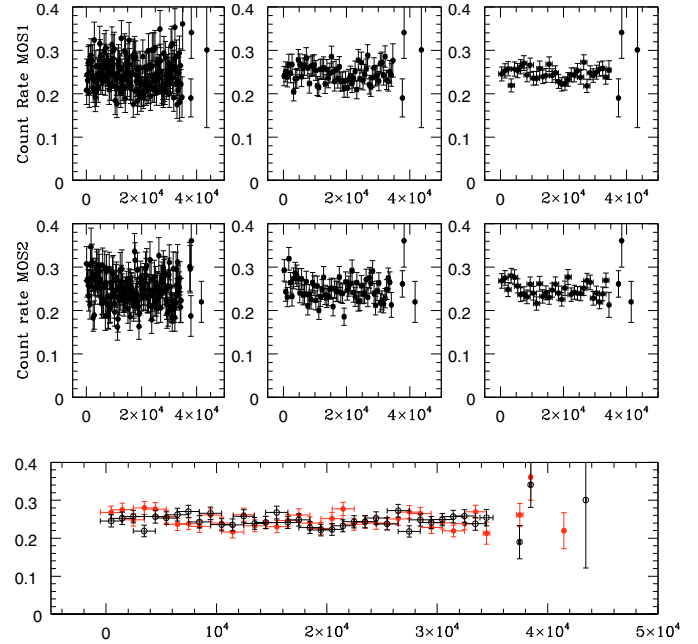


Fig. 1. X-ray lightcurves of θ Car in the 0.2–5 keV band. *Top:* MOS1 lightcurves with time bins of 200, 500 and 1000 s (from left to right). *Middle:* same for MOS2. *Bottom:* superposition of the MOS1 (open black symbols) and MOS2 (filled red symbols) lightcurves with 1 ks-bins.

show that the majority of the flux is clearly confined to 0.1–2 keV, confirming the softness of the source.

The thermal nature of the source is further revealed by the presence of lines, without any significant continuum, in the RGS spectra. These lines are triplets from He-like ions (Ne IX, N VI, and O VII), Lyman lines from H-like ions (Ne X, N VII, and O VIII) and features associated with ionized iron. Their emissivities peak at temperatures of 1.4–5.8 MK (0.12–0.50 keV). A striking characteristic of the spectrum of θ Car is readily derived from a visual comparison of the line strengths with those of “normal” OB stars (see e.g. ζ Ori in Fig. 1 of Pollock 2007): the nitrogen lines appear much stronger while the oxygen and neon lines are weaker. In this context, it should be noted that the carbon line at 33.7 \AA and the magnesium line at 9.2 \AA are below our detection level. Finally, the X-ray lines appear relatively narrow: $FWHM \sim 1000$ km s^{-1} for O VIII Ly α λ 18.97 \AA and N VII Ly α λ 24.78 \AA , ~ 700 km s^{-1} for N VII Ly β λ 20.91 \AA , i.e. the observed line width is mainly instrumental and does not reflect the intrinsic line width (also see results of the fits below).

The EPIC MOS spectra present two broad maxima, at about 0.45 keV and 0.8 keV. While one might then expect the presence of two dominant temperatures, these two peaks actually correspond to the two main groups of lines as revealed by RGS data (strong N lines at long wavelengths for the lower-energy peak and numerous ONeFe lines for the other one). A fit to these data with a differential emission measure model (DEM, *c6pvmkl*, Lemen et al. 1989; Singh et al. 1996) yields only one single, broad thermal component with a peak at 0.2 keV, and an interval of the temperature distribution at half maximum between 0.15 and 0.5 keV, in close agreement with the peak emissivity temperatures (see above).

Unfortunately, the *mekal* model cannot reproduce well the exact rest wavelengths of the X-ray lines, as is obvious from a comparison with the high-resolution data, and we must therefore

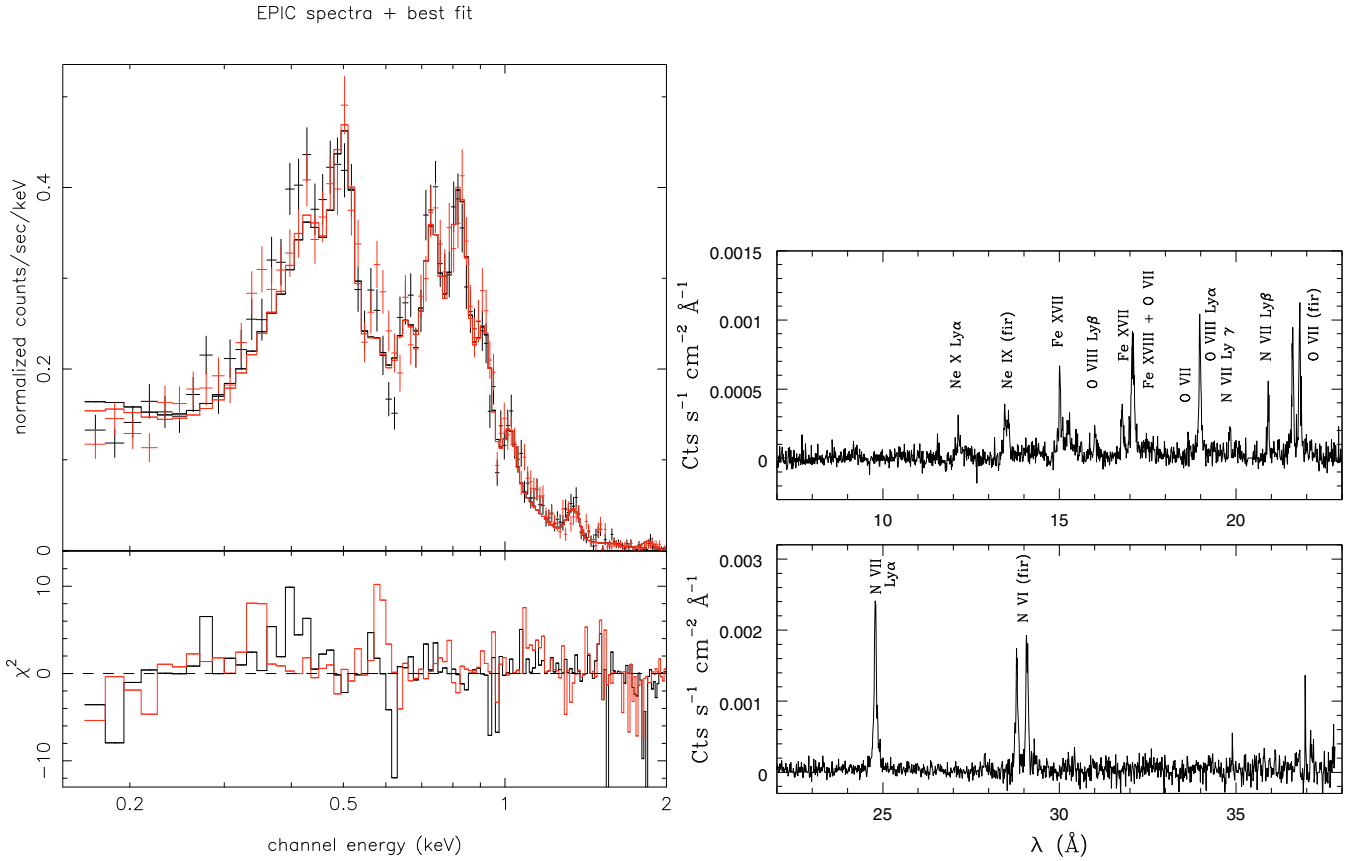


Fig. 2. *Left:* EPIC MOS spectra of θ Car with the best-fit RGS+EPIC model superimposed (see Table 1 – MOS1 appearing in black, MOS2 in red). *Right:* fluxed RGS spectrum of θ Car (from task RGSFLUXER, RGS1+2, orders 1+2) with the main lines identified. Note that the scales of the y-axis differ by a factor of 2 between the upper and lower panels.

rely on the more recent and more precise *apec* model. Since no DEM model of the *apec*-type is available in XSPEC, we tried to fit the spectra with single temperature components. For EPIC MOS data, an absorbed 1T fit does not yield $\chi^2 < 2$ but absorbed 2T models give good results (absorbed 3T models do not yield any significant improvement of the fits). Since lines of NONeFe are clearly detected while conspicuous lines of C and Mg are absent, we let the abundances of these 6 elements vary. We fixed the other abundances to the solar value since no strong constraining information (presence/absence of lines) can be derived from the data. In addition, the absorbing column was fixed to the interstellar value derived in the UV ($1.8 \times 10^{20} \text{ cm}^{-2}$, [Diplas & Savage 1994](#)) since the free- N^{H} fits do not suggest any significant additional, circumstellar absorption. For RGS data, both 1T and 2T yield acceptable residuals. In addition to varying the usual *apec* parameters, two trials were attempted. First, varying the redshift parameter in order to reproduce a global velocity shift: the best fit was found for positive velocities of $+60$ – 100 km s^{-1} , values which are insignificant given the RGS resolution (see also below). Second, reproducing a significant intrinsic width of the lines by convolving the *apec* model with a Gaussian (*gsmooth* model): no significant intrinsic width could be found, reinforcing our conclusion of line widths being mainly instrumental in nature for θ Car.

The parameters of the best-fit models are listed in Table 1. To interpret these results, some facts must be kept in mind: (1) the RGS data are the most sensitive to abundance variations since the lines are resolved for these spectra whereas the line blends

observed in EPIC may yield unrealistic values in some cases (see e.g. the case of carbon¹); (2) the EPIC data are the best to constrain the absorbing column and high-temperature components. Overall, the results of the fits are twofold. On the one hand, the fitted temperatures are low ($0.15 + 0.4 \text{ keV}$ or 0.24 keV). No hard tail is present, nor is any high temperature: this rules out any significant contamination by a putative close PMS star (like in the case of β Cru D, [Cohen et al. 2008](#)) or from the low-mass companion (for a review of the X-ray emission of solar-like stars, see [Güdel 2007](#)). On the other hand, abundances are clearly non-solar: N enhanced by at least a factor of 2, C at only a few percent of the solar values, ONeFe depleted (though to a lesser extent than carbon) – the case of magnesium unfortunately appears unclear due to erratic results. This abundance pattern measured in the RGS data is close to the results derived from the visible spectrum (see Table 2).

The unabsorbed flux (i.e. the flux corrected for the interstellar absorption) measured in the RGS+MOS model amounts to $3.8 \times 10^{-12} \text{ erg cm}^{-2} \text{ s}^{-1}$ in the 0.1–10 keV energy band or $1.6 \times 10^{-12} \text{ erg cm}^{-2} \text{ s}^{-1}$ in the 0.5–10 keV energy band, resulting in luminosities of $1.1 \times 10^{31} \text{ erg s}^{-1}$ and $4.4 \times 10^{30} \text{ erg s}^{-1}$, respectively, for a distance of 152 pc ([Robichon et al. 1999](#)). For the 0.5–10 keV energy range, this converts into a $\log(L_X/L_{\text{BOL}})$

¹ Indeed, a large overabundance in carbon, as derived from the EPIC MOS fits alone, would result in the presence of a strong carbon line at 35 Å, which is not observed in the RGS data.

Table 1. Best-fit models and X-ray fluxes at Earth for θ Car. For each parameter, the lower and upper limits of the 90% confidence interval (derived from the `ERROR` command under `XSPEC`) are noted as indices and exponents, respectively. The normalisation factors are defined as $10^{-14} \int n_e n_H dV / 4\pi D^2$, where D , n_e and n_H are respectively the distance to the source, the electron and proton density of the emitting plasma; the abundance parameters are ratios of the abundance by number (with respect to hydrogen) between the observed spectrum and the solar value. The models are of the type $wabs \times vapec$ or $wabs \times (vapec + vapec)$, with N^H fixed to $1.8 \times 10^{20} \text{ cm}^{-2}$ (Diplas & Savage 1994). The observed fluxes are given in the 0.5–10 keV band and in units $10^{-12} \text{ erg cm}^{-2} \text{ s}^{-1}$.

Instr.	kT_1 keV	norm ₁ 10^{-4} cm^{-5}	kT_2 keV	norm ₂ 10^{-4} cm^{-5}	C	N	O	Ne	Mg	Fe	χ_r^2 (d.o.f.)	f_X^{abs}
MOS1+2	0.15 _{0.14} ^{0.16}	9.10 _{7.12} ^{10.8}	0.36 _{0.35} ^{0.38}	7.30 _{5.56} ^{9.35}	2.27 _{1.56} ^{3.37}	5.04 _{4.17} ^{6.43}	0.36 _{0.29} ^{0.47}	1.19 _{0.95} ^{1.52}	1.23 _{0.95} ^{1.62}	0.96 _{0.78} ^{1.22}	0.40 (1300)	1.48
RGS 1+2	0.24 _{0.24} ^{0.25}	28.4 _{23.6} ^{32.8}	0.04 _{0.0} ^{0.12}	0.00 _{0.0} ^{0.09}	2.32 _{1.93} ^{2.90}	0.10 _{0.08} ^{0.12}	0.38 _{0.31} ^{0.50}	2.47 _{1.19} ^{4.07}	0.61 _{0.50} ^{0.78}	1.85 (594)	1.20	
RGS 1+2	0.16 _{0.15} ^{0.22}	6.84 _{4.92} ^{23.2}	0.39 _{0.37} ^{0.41}	16.0 _{5.97} ^{19.2}	0.00 _{0.0} ^{0.09}	3.85 _{2.98} ^{4.99}	0.19 _{0.10} ^{0.25}	0.40 _{0.30} ^{0.51}	0.83 _{0.30} ^{1.43}	0.32 _{0.26} ^{0.40}	1.74 (592)	1.35
RGS+MOS	0.16 _{0.15} ^{0.16}	12.8 _{10.9} ^{14.8}	0.32 _{0.31} ^{0.32}	23.1 _{20.2} ^{26.3}	0.05 _{0.0} ^{0.12}	2.32 _{2.13} ^{2.54}	0.12 _{0.11} ^{0.13}	0.40 _{0.36} ^{0.45}	0.51 _{0.42} ^{0.60}	0.38 _{0.34} ^{0.41}	0.93 (1902)	1.44

Table 2. Abundance constraints from optical spectra (adapted from Hubrig et al. 2008). The helium abundance is given as the ratio in numbers with respect to hydrogen whereas the others are given in logarithmic values (hydrogen abundance conventionally being at 12.0 in this case); `XSPEC` solar abundances are those of Anders & Grevesse (1989).

Element	El. Abond. in vis.	El. Abond. in XSPEC	ratio
He	0.083 ± 0.028	0.0977	~1
C	7.16 ± 0.46	8.56	0.04
N	8.56 ± 0.27	8.05	3.24
O	8.38 ± 0.22	8.93	0.28
Si	7.43 ± 0.23	7.55	~1
S	7.32 ± 0.33	7.21	~1

of -7.35^2 , or -6.97 taking into account the 0.1–0.5 keV flux. These ratios are slightly lower than the “canonical” value measured for O and early B stars (-6.9 for the 0.5–10. keV band, Sana et al. 2006): θ Car is thus not a bright X-ray emitter for its class, unlike what sometimes has been claimed.

θ Car was observed by both Einstein and ROSAT. It appears in the 2E catalog (Harris et al. 1994) with an IPC count rate of $0.089 \pm 0.006 \text{ cts s}^{-1}$ and in the RASS bright source catalog (Voges et al. 1999) with a PSPC count rate of $0.42 \pm 0.04 \text{ cts s}^{-1}$. For ROSAT, Cassinelli et al. (1994) further reported a count rate of $0.374 \pm 0.016 \text{ cts s}^{-1}$, a value compatible with the RASS detection³. By folding the best fit RGS+EPIC model through the response matrices of these past facilities, we can estimate the “equivalent” IPC or PSPC count rate of this XMM-Newton observation: 0.119 cts s^{-1} for IPC and 0.326 cts s^{-1} for PSPC. During the XMM-Newton observation, θ Car was thus 30% times brighter than during the IPC exposure (a 5σ variation) and $\sim 20\%$ times fainter than during the PSPC exposures (a 3σ variation). Though θ Car does not present any short-term variability during the 50 ks exposure, some longer-term changes are apparently present and future observations are needed to ascertain their nature: are they truly long-term variations, unrelated to the orbital period, or do they occur during the unobserved part of the orbit?

² A bolometric luminosity of $9.7 \times 10^{37} \text{ erg s}^{-1}$ was derived from $B = 2.54$, $V = 2.78$, $E(B-V) \sim 0.$, a distance of 152 pc, and a bolometric correction of -3.16 . It is compatible with the values found in the literature ($\log [L/L_\odot] = 4.30\text{--}4.54$, Gathier et al. 1981; Vardya 1985; Prinja 1989).

³ Randich et al. (1995) quote $0.299 \pm 0.002 \text{ cts s}^{-1}$ for raster scans but the authors mentioned the discrepancy and suggest the scans may yield more uncertain values.

3.2. Analysis of the X-ray lines

Since there are a few strong, isolated lines recorded on the RGS spectra, we decided to fit these individually using Gaussians (including a constant for the pseudo-continuum) within `XSPEC` and `MIDAS`. The results of these fits can be found in Table 3. First, we focused on single lines of the Lyman series. Shifts detected by individual fits are small – in fact below the detection limit considering the RGS characteristics. They broadly agree with the free-redshift fits (see above), small differences being expected since the Aped and Spex databases are not identical. In addition, no significant asymmetry, or intrinsic broadening ($\sigma_{\text{int}} < 350 \text{ km s}^{-1}$) were detected. Three other strong X-ray lines actually are *fir* triplets of He-like ions, i.e. they are composed of a forbidden line, two close intercombination lines and a resonance line. Thermal plasma models like *apec* were only able to reproduce the *r* component of these triplets. A first fit revealed no significant shift/width variations between the lines, as expected theoretically (the lines being formed under the same physical conditions). Therefore, the intrinsic widths and velocities of the three components were constrained to be equal (as for single lines, they were subsequently found to be undetectable). Narrow, unshifted lines are not common in hot stars and are often considered as unreconcilable with a wind-shock origin for the X-ray emission. Such lines are generally expected for magnetic objects (θ^1 Ori C, τ Sco, Gagné et al. 2005; Mewe et al. 2003), a notable exception being another early B-type star, β Cru, that has narrow lines but no magnetic field (Cohen et al. 2008).

The relative strengths of the *fir* lines depend on the plasma temperature, the plasma density, and the stellar radiation field. More precisely, the *f* line is weakened and the *i* line strengthened when the density or the radiation field is high; for hot stars such as θ Car, the latter has a much stronger impact than the former. On the other hand, the $(f+i)/r$ ratio is sensitive to plasma temperature (for more details see e.g. Porquet et al. 2001). These *fir* lines cannot be reproduced by “simple” `XSPEC` models, as already mentioned, but the Gaussian fits allow us to derive the *f/i* and $(f+i)/r$ ratios. Monte-Carlo simulations, assuming a normal distribution for the line fluxes (90% confidence interval is $\pm 1.645\sigma$), were used to estimate the errors on these ratios.

In contrast with the colliding-wind systems where $f \gg i$ (Pollock et al. 2005), the forbidden lines of θ Car remain undetected in all three triplets (Fig. 3). Therefore, only an upper limit can be derived on the *f/i* ratios: the one-sided 90% confidence interval is 0–0.06 for N VI, 0–0.17 for O VII 0–0.15 for Ne IX. These ratios can then be compared with the values from Porquet et al. (2001) for $T_e = 2.0 \text{ MK}$ (close to the main component at $kT \sim 0.2 \text{ keV}$), $T_{\text{rad}} = 30 \text{ kK}$ (since $T_{\text{eff}} = 31 \pm 1 \text{ kK}$, Hubrig et al. 2008) and dilution factors W of 0.01, 0.10 and

Table 3. Best-fit Gaussians for selected X-ray lines. Rest energies of the lines are taken from the Spex database v2.0 (Kaastra, 2002, private communication). Ly α lines contain two components too close to be disentangled; the velocities given below are calculated with respect to the A component. Emission measures are calculated using emissivities at the mean plasma temperature ($kT = 0.2$ keV, or $\log T = 6.4$) or the maximum emissivities – both being taken from the Spex database.

Ion	E_0 keV	v km s $^{-1}$	σ 10 $^{-4}$ keV	f_X^{abs} 10 $^{-5}$ phot cm $^{-2}$ s $^{-1}$	EM ($kT = 0.2$ keV) 10 53 cm $^{-3}$	EM (max emissivity) 10 53 cm $^{-3}$
<i>H-like lines</i>						
O VIII Ly α	0.653550	-112_{-129}^{+74}	$0.2_{0.}^{61}$	$8.41_{7.20}^{9.63}$	$1.05_{0.90}^{1.20}$	$0.89_{0.76}^{1.01}$
N VII Ly β	0.592940	-24_{-324}^{+235}	$0.6_{0.}^{85}$	$2.73_{1.61}^{4.00}$	$25.3_{14.9}^{37.1}$	$24.2_{14.3}^{35.4}$
N VII Ly α	0.500360	-218_{-223}^{+108}	$0.1_{0.}^{64}$	$24.5_{22.5}^{26.4}$	$21.2_{19.5}^{22.9}$	$18.6_{17.1}^{20.1}$
<i>He-like lines</i>						
Ne IX f	0.90499	-374_{-382}^{+162}	$0.6_{0.}^{53}$	$0.0_{0.}^{24}$	$4.71_{3.43}^{7.44}$	$2.25_{1.64}^{3.55}$
Ne IX i	0.91481			$1.92_{1.25}^{3.40}$		
Ne IX r	0.92195			$2.92_{2.27}^{4.00}$		
O VII f	0.56101	4_{-112}^{+48}	$0.1_{0.}^{68}$	$0.67_{0.}^{1.57}$	$1.25_{0.95}^{1.59}$	$1.08_{0.81}^{1.37}$
O VII i	0.56874			$8.38_{6.65}^{10.0}$		
O VII r	0.57395			$6.73_{5.27}^{8.50}$		
N VI f	0.41986	-34_{-57}^{+43}	$0.0_{0.}^{82}$	$0.1_{0.}^{101}$	$63.3_{55.1}^{73.6}$	$18.0_{15.7}^{20.9}$
N VI i	0.42621			$17.1_{15.1}^{19.3}$		
N VI r	0.43065			$14.4_{12.3}^{16.3}$		

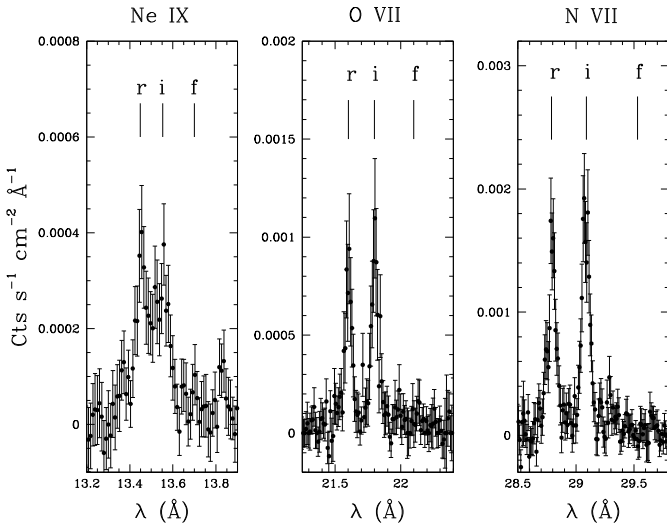


Fig. 3. Zoom on the *fir* triplets recorded in the fluxed RGS spectrum of θ Car. Tickmarks indicate the rest wavelengths of the lines. The line at 13.82 Å belongs to Fe XVII; there is no trace of the Fe XIX line at 13.78 Å that could contaminate the f component of the Ne IX triplet.

0.50: the oxygen and nitrogen ratios do not provide strong constraints (even W values lower than 0.01 are permitted), but the neon triplet favors dilution factors W of ~ 0.5 , i.e. an emission occurring close to the star. Since θ Car and τ Sco display similar stellar parameters (same T_{eff} , gravity, spectral type), we can infer more precise limits by using the f/i evolution calculated by Mewe et al. (2003) and shown in Fig. 2 of that paper: the formation radii are $< 20 R_*$ from the N VI and O VII triplets, but $< 5 R_*$ for the Ne IX triplet. Such values agree well with those found in other hot stars, but they are too loosely constrained to enable us to distinguish between a wind-shock, coronal or magnetic origin for the X-ray emission.

Turning to the $(f+i)/r$ ratio, the values are $1.19_{1.03}^{1.49}$ for N VI, $1.34_{1.01}^{1.90}$ for O VII and $0.66_{0.33}^{1.23}$ for Ne IX, where indices and exponents give the lower and upper limits of the 90% confidence interval. These values are close to one, suggesting that plasma is

collision-dominated (Porquet et al. 2001). Comparison with the theoretical values from Porquet et al. (2001) yields plasma temperatures $\lesssim 1$ MK for N VI and O VII and ~ 6 MK for Ne IX. This indicates that a range of temperatures could exist in the X-ray emitting plasma, as was already suggested by the rather broad peak of the DEM models.

Another independent temperature estimate relies on the ratio of He-like to H-like line fluxes. The lines fluxes were first dereddened before estimating this ratio. For nitrogen, it amounts to 1.41 ± 0.14 if one considers the Lyman α line or 12.6 ± 3.6 for Lyman β . Linearly interpolating the Spex database, such ratios correspond to $\log(T)$ of 6.23 ± 0.02 and 6.25 ± 0.03 , respectively. For oxygen, the He-to-H line ratio amounts to 1.99 ± 0.36 , which yields $\log(T) = 6.37 \pm 0.02$. These temperatures agree well with the results from DEM and *apex* models (see above); they are larger than those derived from the comparison of $(f+i)/r$ ratios and Porquet et al.'s models but discrepancies between these two temperature estimates are often found.

Finally, the observed line fluxes in units $\text{ph cm}^{-2} \text{s}^{-1}$ were dereddened and converted to $\text{erg cm}^{-2} \text{s}^{-1}$, in order to derive the emission measures ($\text{EM} = 4\pi d^2 f^{\text{unabs}} / Q(T_e)$) at a distance of 152 pc. The emissivities $Q(T_e)$ were found in the Spex database, and were summed if several components (like the *fir* lines) exist. Table 3 present the emission measures (EMs) calculated at the mean plasma temperature (~ 0.2 keV) and at the temperature of maximum emissivity. It should be noted that O VII and O VIII lines yield similar EMs, but the value for N VI is three times that of N VII if one considers the mean plasma temperature. However, the discrepancy disappears if one considers peak emissivity temperatures. This might be interpreted once again as a need to drop the too simplistic assumption of having only one plasma temperature: most probably, the X-ray emitting plasma displays a range in temperatures, individual lines being emitted at the best conditions for each one. We will thus only consider the EM values calculated with the maximum emissivities. For solar abundances, all EMs should have similar values; the dispersion of the observed EMs confirms once again the non-solar abundances of θ Car. When dividing the EMs, we find a N/O enhancement of a factor of 20 and a Ne/O ratio of about 2.5, compared to solar values. The global fits, though they could not

reproduce the intense i component of the triplets, confirm these values. The $(N/O)_*/(N/O)_\odot$ ratio is only slightly larger than the value of ~ 12 found by Hubrig et al. (2008). This underlines the good capabilities of the X-ray data for constraining abundances.

4. Conclusions

XMM-Newton observations revealed the atypical character of θ Car. Overall, its X-ray emission appears very soft as well as rather weak. Almost all the flux is found below 1 keV; indeed, spectral fits indicate a dominant temperature of about 0.2 keV. The total unabsorbed luminosity in the 0.1–10 keV range amounts to 1.0×10^{31} erg s $^{-1}$, which yields a L_X/L_{BOL} ratio slightly lower than the ‘canonical’ value for OB stars. Though no significant variability is detected during the 50 ks XMM-Newton observation, an increase (resp. decrease) of the flux is clearly observed compared to previous Einstein (resp. ROSAT) observations.

The high-resolution spectrum of θ Car, revealed by the RGS, does not show any significant continuum emission but is solely composed of lines of H- and He-like ions of N, O, and Ne as well as some iron lines. To the resolution limits of the RGS, these lines appear narrow and unshifted: the observed width of these lines is mainly instrumental and the intrinsic width is limited to < 350 km s $^{-1}$. The nitrogen lines are anomalously strong: the spectral fits reveal a large enrichment in nitrogen (abundance 3 times solar), together with a strong deficit in carbon, which both agree well with the values found in the optical spectrum (Hubrig et al. 2008). Neon, oxygen and iron also appear slightly depleted in the X-ray spectrum. For the *fir* triplets, the forbidden component is fully suppressed while the intercombination lines are slightly stronger than the resonance component. The f/i ratios suggests a formation radius rather close to the star, below 5 stellar radii.

With its soft X-ray spectrum and its narrow X-ray lines, θ Car clearly appears different to O-type stars. Comparing θ Car to other B-type objects with high-resolution spectra, we find that the temperature distribution is quite typical of “normal” B stars: the DEM is similar to that of ϵ Ori and only slightly broader than for β Cru and Spica (Zhekov & Palla 2007). Similar temperatures, fluxes and overall line properties were also found in a detailed analysis of β Cru (Cohen et al. 2008), though in the latter case, more precise constraints could be found on the formation radius. On the other hand, θ Car seems

very different from τ Sco as far as softness, abundances, and flux level are concerned, but both objects present unshifted, narrow X-ray lines (Mewe et al. 2003; Cohen et al. 2003). Such lines are at odds with the wind-shock model, though it is still unclear how this model could apply in the case of low mass-loss rates, such as those of B-type stars. Actually, narrow lines are often attributed to magnetic confinement. However, this process is still uncertain for θ Car, as magnetic field searches have been inconclusive thus far (Hubrig et al. 2008). As for β Cru, additional observations, especially polarimetric ones, are needed before θ Car can be fully understood and the origin of its X-ray emission pinpointed.

Acknowledgements. We acknowledge support from the Fonds National de la Recherche Scientifique (Belgium) and the PRODEX XMM and Integral contracts. We thank S. Hubrig for giving us the opportunity to read her paper before acceptance, and T. Morel for useful discussions.

References

- Anders, E., & Grevesse, N. 1989, *Geochim. Cosmochim. Acta*, 53, 197
 Borra, E. F., & Landstreet, J. D. 1979, *ApJ*, 228, 809
 Cassinelli, J. P., Cohen, D. H., MacFarlane, J. J., Sanders, W. T., & Welsh, B. Y. 1994, *ApJ*, 421, 705
 Cohen, D. H., de Messières, G. E., MacFarlane, J. J., et al. 2003, *ApJ*, 586, 495
 Cohen, D. H., Kuhn, M. A., Gagné, M., Jensen, E. L. N., & Miller, N. A. 2008, *MNRAS*, 386, 1855
 Diplas, A., & Savage, B. D. 1994, *ApJS*, 93, 211
 Gagné, M., Oksala, M. E., Cohen, D. H., et al. 2005, *ApJ*, 628, 986
 Gathier, R., Lamers, H. J. G. L. M., & Snow, T. P. 1981, *ApJ*, 247, 173
 Güdel, M. 2007, *Living Rev. Sol. Phys.*, 4, 3
 Harris D. E., et al. 1994, *SAO HEAD CD-ROM Series I (Einstein)*, Nos. 18–36
 Hubrig, S., Briquet, M., Morel, T., et al. 2008, *A&A*, 488, 287
 Lemen, J. R., Mewe, R., Schrijver, C. J., & Fludra, A. 1989, *ApJ*, 341, 474
 Lloyd, C., Stickland, D., & Walborn, N. R. 1995, *PASP*, 107, 1030
 Mewe, R., Raassen, A. J. J., Cassinelli, J. P., et al. 2003, *A&A*, 398, 203
 Pollock, A. M. T. 2007, *A&A*, 463, 1111
 Pollock, A. M. T., Corcoran, M. F., Stevens, I. R., & Williams, P. M. 2005, *ApJ*, 629, 482
 Porquet, D., Mewe, R., Dubau, J., Raassen, A. J. J., & Kaastra, J. S. 2001, *A&A*, 376, 1113
 Prinja, R. K. 1989, *MNRAS*, 241, 721
 Randich, S., Schmitt, J. H. M. M., Prosser, C. F., & Stauffer, J. R. 1995, *A&A*, 300, 134
 Robichon, N., Arenou, F., Mermilliod, J.-C., & Turon, C. 1999, *A&A*, 345, 471
 Sana, H., Stevens, I. R., Gosset, E., Rauw, G., & Vreux, J.-M. 2004, *MNRAS*, 350, 809
 Sana H., Rauw G., Nazé Y., Gosset E., & Vreux J.-M. 2006, *MNRAS*, 372, 661
 Singh, K. P., White, N. E., & Drake, S. A. 1996, *ApJ*, 456, 766
 Vardya, M. S. 1985, *ApJ*, 299, 255
 Voges, W., Aschenbach, B., Boller, Th., et al. 1999, *A&A*, 349, 389
 Zhekov, S. A., & Palla, F. 2007, *MNRAS*, 382, 1124